NJC

PAPER

View Article Online
View Journal | View Issue

Cite this: *New J. Chem.*, 2016, **40**, 1213

The synthesis and characterization of tributyl phosphate grafted carbon nanotubes by the floating catalytic chemical vapor deposition method and their sorption behavior towards uranium

Shruti Mishra,[ab] Jaya Dwivedi,[b] Amar Kumar[c] and Nalini Sankararamakrishnan*[a]

Received (in Montpellier, France) 28th September 2015,
Accepted 18th November 2015

DOI: 10.1039/c5nj02639c

www.rsc.org/njc

Carbon nanotubes (CNTs) were synthesized by the floating catalytic chemical vapor deposition technique using ferrocene in benzene as the hydrocarbon source. The functionalization of CNTs was carried out by oxidation (CNT-OX) and grafting with a tributyl phosphate (TBP) ligand (CNT-TBP). Various spectroscopic techniques including scanning electron microscopy (SEM), Fourier Transform Infra Red Spectroscopy (FTIR), BET surface area and X-ray photoelectron spectroscopy (XPS) were used to characterize the adsorbents. FTIR and XPS studies revealed the efficient grafting of the TBP ligand on the CNT surface. The effect of the initial pH and the contact time for the maximum adsorption of U(VI) with CNT-plain, CNT-OX and CNT-TBP was studied. The spontaneity of the sorption was confirmed by thermodynamic data. A pseudo second order model with a regression coefficient of >0.978 was obtained for CNT-TBP and equilibrium was reached within 3 h. The Langmuir maximum adsorption capacity of U(VI) at pH 5 for CNT, CNT-OX and CNT-TBP was found to be 66.6, 100.0 and 166.6 mg g^{-1} respectively. Using 0.1 M HCL as a desorbent, recyclability studies were carried out for three cycles. The probable mechanism of adsorption between U(VI) and CNT-TBP could be understood through FTIR and XPS techniques.

1. Introduction

Advanced treatment methods are required for the management of radioactive waste produced by nuclear power plants.[1,2] Uranium is one of the major waste materials in spent nuclear fuels or mine tailings, and it can cause significant contamination.[3] An exposure level of 0.1 mg kg^{-1} of body weight of natural U could result in kidney damage.[4] The World Health Organization's guideline value for uranium is set at 50 μg L^{-1}.[5] Several methods have been found to be useful for the removal of uranyl ions from process effluents and wastewater. For water treatment, compared to other techniques adsorption has been found to be a preferred technique owing to its flexibility, cost effectiveness, ease of operation and simple design. A weak affinity and low adsorption capacity are exhibited by natural adsorbents for U(VI) under ambient conditions. Therefore, there is a need for new, eco-friendly and economical adsorbents with high adsorption capacities and stronger chemical interaction towards U(VI). Among the various adsorbents reported in the literature, sorption materials made of carbon offer a variety of advantages including high thermal and radiation resistance and improved chemical stability under acidic conditions compared to other inorganic sorbents and ion exchange resins.[6] Various carbonaceous materials like activated carbon,[7,8] activated carbon fibers,[9] carbon nanotubes[10,11] and mesoporous carbon[12] have been reported for the removal of U(VI) ions from aqueous solution. Tributyl phosphate (TBP) is one of the widely used extractants for the removal of U(VI).[13] Thus, in this work three kinds of carbon nanotubes namely plain CNTs, oxidized CNTs and TBP grafted CNTs structurally characterized by various techniques will be prepared and evaluated for the removal and recovery of U(VI). Using spectroscopic tools the adsorption mechanism between U(VI) and CNT-TBP will also be discussed.

2. Materials and methods

All reagents and chemicals like nitric acid (HNO_3), sodium hydroxide (NaOH), tributyl phosphate (TBP), uranyl(VI) nitrate ($UO_2(NO_3)_2 \cdot 6H_2O$), solvents (ethanol, acetone) and other reagents

[a] *Centre for Environmental Science and Engineering, Indian Institute of Technology Kanpur, Kanpur, U.P. 208016, India. E-mail: nalini@iitk.ac.in; Tel: +91-5122596360*
[b] *Department of Chemistry, Banasthali Vidyapith, Rajasthan 304022, India*
[c] *Bhabha Atomic Research Centre, Trombay, Mumbai, India*

used in this study are of analytical grade. Using Milli-Q purified water (resistivity >18.2 MΩ cm) the reagents and standards were prepared.

2.1 Preparation of carbon nanotubes

Carbon nanotubes were prepared by the floating catalyst horizontal chemical vapour deposition technique using 2% ferrocene in benzene as the hydrocarbon source.[14] The flow rate of the ferrocene/benzene solution and nitrogen gas was controlled using a peristaltic pump and a mass flow controller (Bronkhorst high-tech. Netherlands), respectively. The temperature of the electric furnace was gradually increased to 800 °C under a nitrogen atmosphere. The flow rates of the ferrocene/benzene solution and nitrogen gas were set to 1 mL min^{-1} and 100 sccm respectively and the ferrocene/benzene solution was pumped into the reactor for 30 min at an 800 °C reactor temperature. The reactor was gradually cooled to room temperature. The deposited CNTs were removed and used for further experiments.

2.2 Preparation of CNT-OX

Around 1 g of plain CNTs was heated with 10 ml of nitric acid at 80 °C until the acid evaporated completely. Then, a thorough washing with distilled water was carried out until the pH of the filtrate became neutral. Finally, the obtained product was dried in an oven at 70 °C overnight and used for further experiments.

2.3 Preparation of CNT-TBP

One gram of CNT-OX was treated with 20 mL of tributyl phosphate and the solution was sonicated for 24 h. Then, the obtained mixture was washed using distilled water and dried at 70 °C overnight and used for further experiments.

The preparation of CNT-OX and CNT-TBP is shown in Scheme 1.

2.4 Batch studies

Using batch mode, sorption experiments were carried out by equilibrating 20 mL of 100 mg L^{-1} of uranyl ions at pH 5 for 3 h using 0.05 g of the adsorbent. The concentration of uranyl ions in the aqueous phase was analyzed by inductive coupled plasma-mass spectrometry (ICP-MS) (Thermo Scientific, XSERIES 2). The amount of uranyl ions adsorbed (mg) per unit mass of the adsorbent (g), q_e, was obtained by the equation given below:

$$q_e = \frac{(C_i - C_e)}{m} \times V \quad (1)$$

where C_i and C_e are the initial and equilibrium concentrations of uranyl ions (mg L^{-1}), V is the volume of the aqueous phase (L), and m is the dry mass of the adsorbent (g). Kinetic experiments were conducted by monitoring the amount of uranyl ions adsorbed at regular time intervals. The amount of U(VI) adsorption at temperatures 25 °C, 35 °C and 45 °C was measured for calculating the thermodynamic parameters. The recyclability of CNT-TBP was investigated using 0.1 M HCl as a desorber.

2.5 Instrumentation

Fourier Transform Infra-Red (FTIR) measurements were recorded on a Tensor 27 (Bruker, Germany) in the attenuated total reflectance (ATR) mode. SEM micrographs were acquired using an FEI Quanta 200 machine. TEM analysis was carried out on a Technai G2 T-20 (FEI, Eindhoven, Netherlands) transmission electron microscope operated at 200 kV. Using a PHI 5000 Versa Prob II (FEI Inc.) spectrometer with non-monochromatic Al Kα radiation (1486.6 eV), XPS measurements were carried out. Individual spectral peaks were deconvoluted using XPSPEAK41 software. For fitting the spectral region a nonlinear Shirley background subtraction was applied. The surface characteristics of the sorbent namely pore size distribution (PSD),

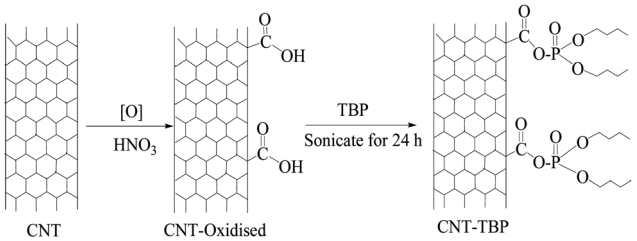

Scheme 1 Preparation of CNT-OX and CNT-TBP.

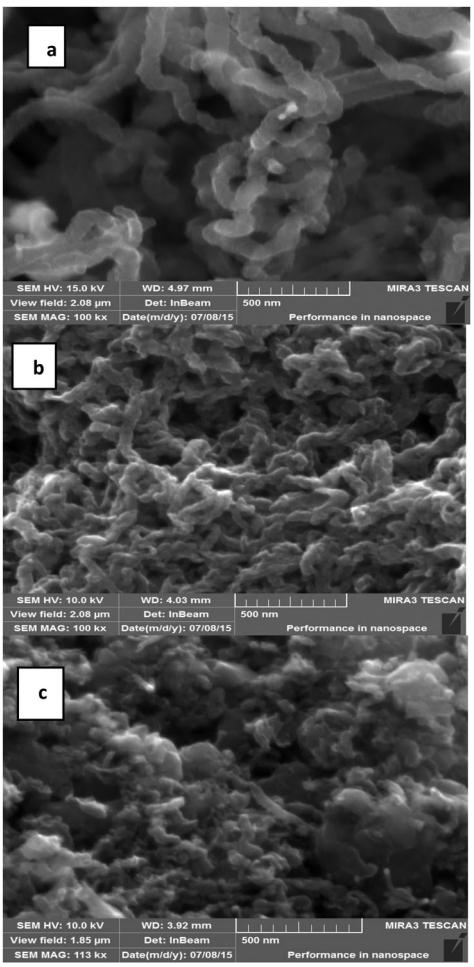

Fig. 1 SEM images of (a) CNT-plain, (b) CNT-OX and (c) CNT-TBP.

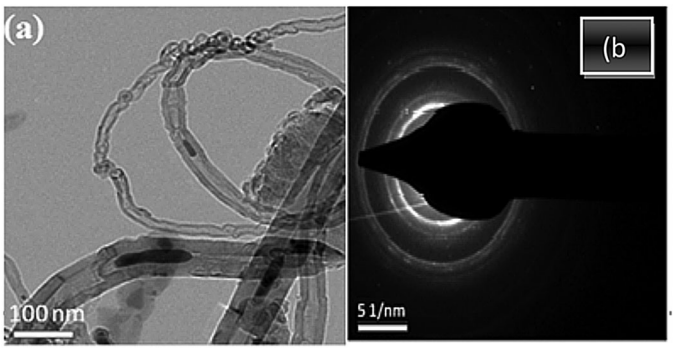

Fig. 2 TEM images of CNT-plain at (a) 100 nm magnification and (b) electronic diffraction spectra.

pore volume and specific surface area were measured using an Autosorb-1C instrument (Quantachrome, USA). Finally, the concentration of U(VI) in the aqueous solutions was determined by inductive coupled plasma mass spectroscopy (ICP-MS; Thermo, X-Series2).

3. Results and discussion

As described in the Materials and methods section, initially CNTs were synthesized by the floating catalytic chemical vapour deposition method and grafting was carried out by oxidation (CNT-OX) and further treatment with tributyl phosphate (CNT-TBP). Thus the prepared adsorbents *viz.*, CNT-plain, CNT-OX and CNT-TBP were characterized by various techniques including SEM, TEM, BET surface analysis, FTIR, and XPS and evaluated for their applicability towards the removal of uranyl ions.

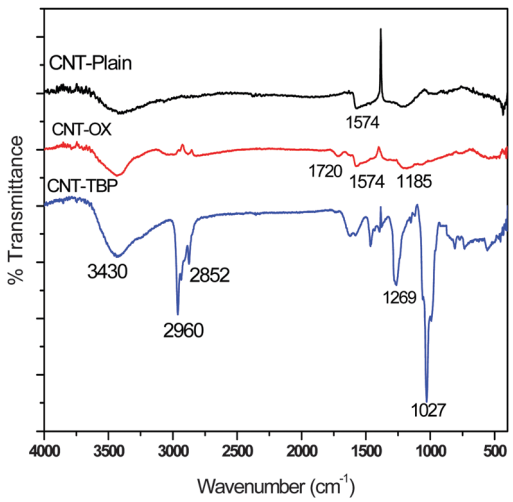

Fig. 3 FTIR spectra of CNT-plain, CNT-OX and CNT-TBP.

3.1 Characterization of adsorbents

3.1.1 Surface morphology using SEM and TEM. SEM images of plain CNTs, oxidized CNTs, and CNT-TBP are shown in Fig. 1(a)–(c) respectively. The diameter and length of the prepared CNTs were found to be in the range of 20–80 nm and 1–10 μm respectively (Fig. 1(a)). In CNT-OX (Fig. 1(b)) exfoliated rope like structures are observed. This could be attributed to the etching of graphitic layers of CNTs during oxidation. After oxidation and grafting of the TBP ligand (Fig. 1c) there was no appreciable difference in the surface characteristics which confirms that minimal damage occurred after grafting with the TBP ligand. The HR-TEM image revealed the presence of nanotubes and iron particles located inside the nanotubes (Fig. 2(a)). The corresponding diffraction rings and a bright spot in the electron diffraction pattern (Fig. 2(b)) suggest that the obtained CNTs possess crystalline Fe particles.

3.1.2 FTIR analysis of the prepared sorbents. FTIR spectra of CNT-plain, CNT-OX and CNT-TBP are shown in Fig. 3. A broad peak at ~3430 cm^{-1} is due to the O–H stretch frequency of the hydroxyl group (Fig. 3). The spectra of CNT-OX show peaks at 1720 cm^{-1} and 1185 cm^{-1}, which are associated with the asymmetric C=O and C–O stretching band of the carboxylic acid (–COOH) group.[15] The peak observed at 1574 cm^{-1} is related to the carboxylate anion stretch mode. The spectrum of CNT-TBP presents the C–H bond stretching at around 2960 cm^{-1} due to methyl groups on MWCNTs. The signal at 2852 cm^{-1} can be assigned to the symmetric stretching of $-CH_2-$ groups of the tributyl phosphate moiety. Furthermore, in CNT-TBP, the P=O stretching vibration, occurred at 1269 cm^{-1}. The P–O–C vibration occurred at 1027 cm^{-1},[16] which proves the grafting of TBP on the CNT surface.

3.1.3 Surface area, pore volume and pore size distribution analysis using BET measurements. The surface characteristics of the plain CNTs, CNT-OX and CNT-TBP were obtained by the standard BET method in a relative pressure range from 0.05 to 0.35. The nitrogen adsorption–desorption isotherm of CNT-plain is shown in Fig. 4. The material exhibited a type IV behaviour typical of a mesoporous material. The total pore volume, meso, micro and macro pore volumes, were calculated using Quantochrome's software. The surface characteristics of various sorbents prepared are listed in Table 1. It is evident from the data that the prepared sorbents possessed a small pore size and a large surface area which lead to strong confinement of the adsorbed analyte on the surface of the CNTs. Upon oxidation with nitric acid, the specific surface area increased from 99.8 $m^2\ g^{-1}$ to 111.9 $m^2\ g^{-1}$, which could be attributed to the opening of pores. Further CNT-TBP exhibited a marginal decrease in the surface area which is due to the anchoring of the TBP ligand.

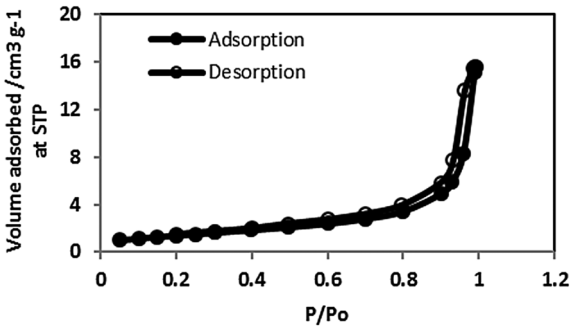

Fig. 4 Nitrogen adsorption isotherm of CNT-plain.

Table 1 Surface characteristics of various prepared CNTs

Adsorbent	Surface area (m^2 g^{-1})	Average diameter (nm)	Total pore volume (cm^3 g^{-1})	Pore volume (cm^3 g^{-1})	
				Meso	Micro
CNT-plain	99.81	14.67	0.3661	0.4280	0.0048
CNT-OX	111.89	10.52	0.2943	0.1681	0.0049
CNT-TBP	102.77	18.90	0.4861	0.4197	0.0043

3.2 Mechanism of interaction between the sorbent and the sorbate using XPS and FTIR studies

To study the interaction of U(VI) with CNT-TBP, XPS spectra were recorded for CNT-TB and CNT-TBP-U. Fig. 5 illustrates the O 1s, C 1s, P 2p and U 4f spectra. Uranium loading is observed in CNT-TBP-U evidenced by the appearance of doublet peaks of U $4f_{5/2}$ and U $4f_{7/2}$ with a splitting value of 10.72 eV. Table 2 depicts the binding energies of O 1s, C 1s, P 2p and the splitting values of the U(VI) spectra. To get a further insight into the U(VI) sorption, the core level scans for C 1s, O 1s, P 2p, and U 4f on CNT-TBP and CNT-TBP-U were analyzed.

The O 1s and C 1s spectra of CNT-TBP and CNT-TBP-U are shown in Fig. 6. The peak fitting results of the C 1s, O 1s, P 2p, U 4f, before and after U(VI) loading on CNT-TBP are shown in Table 2. From Fig. 6a, the three main components of the O 1s spectra occurred at 531.54, 533.56 and 532.87 eV, respectively,

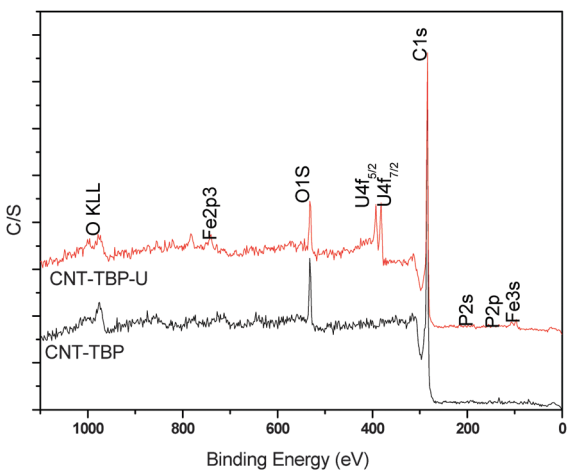

Fig. 5 XPS survey scans of plain and U(VI) loaded CNT-TBP systems.

Table 2 Binding energies (eV) of CNT-TBP before and after uranium sorption

Adsorbent	C 1s	O 1s	P 2p	U 4f5/2	U 4f7/2	Splitting value
CNT-TBP	284.55	532.02	133.76	—	—	
CNT-TBP-U	283.65	532.47	133.97	392.87	382.15	10.72

Table 3 Molecular level binding energies of CNT-TBP and CNT-TBP-U systems

Core levels	CNT-TBP			CNT-TBP-U		
	Binding energy (eV)	FWHW (eV)	Area	Binding energy (eV)	FWHW (eV)	Area
C 1s	285.06	0.674	1575.04	285.87	1.25	1202.25
	284.58	0.440	3307.22	284.91	0.61	1725.39
	284.25	0.484	7563.98	284.16	0.45	4136.41
	286.03	1.590	1971.61	284.46	0.43	3907.03
O 1s	531.54	2.318	3263.12	531.06	1.51	1944.42
	533.56	0.890	241.96	533.21	1.07	529.58
	532.87	1.073	839.65	531.76	1.79	211.65
				532.29	1.22	717.02
P 2p	133.40	1.184	148.30	133.95	1.41	121.28
	134.30	1.099	82.31	134.52	1.50	12.60
	—	—	—	133.12	0.87	38.65
U 4f7/2	—	—	—	381.05	1.72	990.30
	—	—	—	382.13	1.91	1717.22

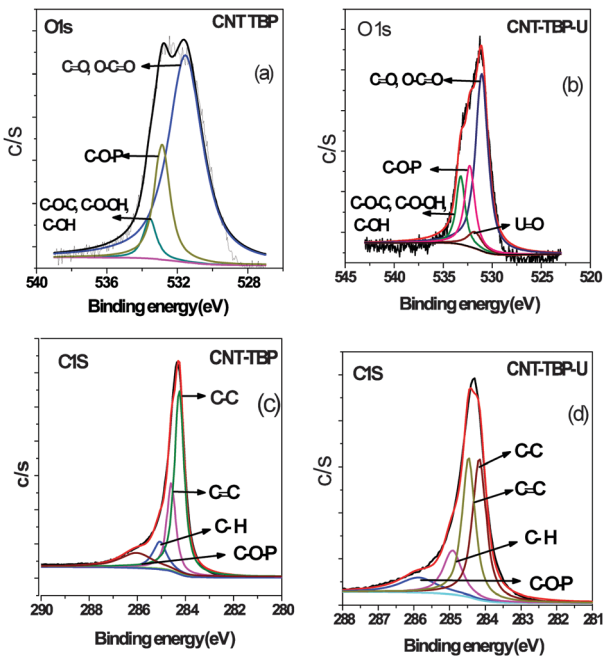

Fig. 6 Curve fitted high resolution scans of (a) O 1s of CNT-TBP, (b) O 1s of CNT-TBP-U, (c) C1s of CNT-TBP and (d) C 1s of CNT-TBP-U.

corresponding to C═O, O–C═O and C–O–C, C–O–OH, C–OH[17] and C–O–P.[18] Thus the data confirm the grafting of the TBP ligand onto the CNT surface. After U(VI) loading (Fig. 6b), peaks occurred at 531.06, 532.21, 531.76, and 532.29 eV.

The presence of the U═O bond is confirmed by the appearance of an additional peak after U(VI) sorption.[19,20] Furthermore, after U(VI) adsorption O 1s binding energies were shifted to lower values. This further confirms that complexation occurs between the oxygen-containing tributyl phosphate groups and uranyl ions during adsorption.

Fig. 6c and d shows the molecular level C 1s of CNT-TBP and CNT-TBP-U respectively. The four individual component peaks of C 1s occurred at 284.25, 284.58, 285.06 and 286.03 eV corresponding to C–C, C═C, C–H and C–O–P[17,18] bonds respectively. After uranyl adsorption the peaks shifted to lower binding energies owing to the complexation of the tributyl phosphate group and U(VI) ions.

Fig. 7a and b denotes the P 2p spectra of CNT-TBP before and after loading U(VI) respectively. In CNT-TBP, the binding energy of the P $2p_{3/2}$ component was found at 134.3 eV: the P 2p spectrum is a convolution of the P $2p_{1/2}$ and P $2p_{3/2}$ peaks that were resolved, keeping their branching ratio and their difference equal to 0.9 and 1.8 eV, respectively. After uranium sorption (Fig. 7b) the shifting of peaks to higher binding energies was observed. Additionally a new peak was observed at 133.21 eV, which could be attributed to the P–O–U bond.

The U $4f_{7/2}$ spectrum (Fig. 7c) was deconvoluted into two components: the peak corresponding to the free uranyl ion that occurred at 381.05 eV and the peak of covalently bonded oxygen and U(VI) that occurred at 382.13 eV (Table 3).

From the above discussion it is clear that the TBP ligand is grafted onto CNTs and complexation of uranyl ions occurred with the phosphoryl group of the tributyl phosphate ligand.

Infra red spectra of CNT-TBP before and after U(VI) sorption are shown in Fig. 8. It is evident from the figure that, after U(VI) sorption, a shift in P═O vibration band to 1110 cm^{-1} was observed. This could be attributed to the coordination of UO_2^{2+}

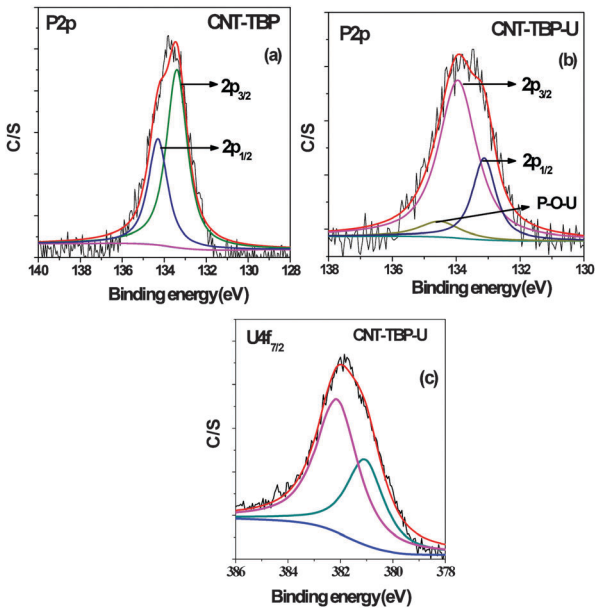

Fig. 7 Curve fitted high resolution scans of (a) P 2p of CNT-TBP (b) P 2p of CNT-TBP-U (c) U $4f_{7/2}$ of CNT-TBP-U.

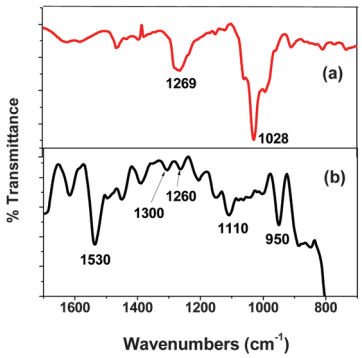

Fig. 8 FTIR scans of (a) CNT-TBP and (b) CNT-TBP-U.

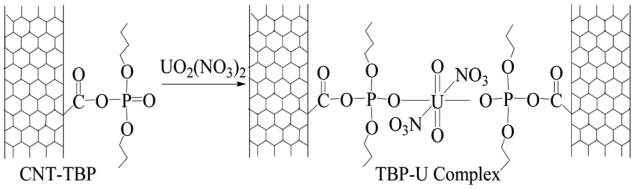

Scheme 2 Schematic representation of U(VI) loading on CNT-TBP.

cations with the P–O bond of the TBP molecule. The shift of the P═O frequency after U(VI) sorption was about 82 cm^{-1}, and the magnitude of the frequency shift obtained was consistent with other uranyl complexes with organophosphorus ligands.[21,22] The mode of nitrate complexation to the metal ion can be determined by the separation $\Delta\nu$ of the symmetric $\nu1$ and asymmetric $\nu2$ NO_2 stretching frequencies.[23–25] A $\Delta\nu$ value >186 cm^{-1} indicates a bidentate chelate environment, while a value ≤ 115 cm^{-1} indicates a monodentate coordination. It is evident from the spectra that $\Delta\nu = 270$ cm^{-1} ($\nu1$ at 1300 cm^{-1} and $\nu2$ at 1530 cm^{-1}) was obtained which indicated a bidentate chelation of the nitrate ion to the uranyl ion. Further an additional vibration occurred at 950 cm^{-1} which could be assigned to the asymmetric stretching frequency of the U═O bond.[26] Based on the above discussions the following reaction scheme has been proposed (Scheme 2) for the sorption of the uranyl ion and CNT-TBP.

3.3 The effect of initial pH on sorption

The initial pH of the solution containing 100 mg L^{-1} of uranyl ions was varied from 2 to 8 and equilibrium experiments were carried out (Fig. 9). The amount of uranyl ions adsorbed increased from pH 4 to 6 and a further increase in pH resulted in decreased sorption. The adsorption trends observed over the pH range studied could be assigned to the distribution of various uranyl species. It is well known that at pH values ≤ 3, UO_2^{2+} is the predominant species[11] and in the pH range of 4.0–9.0 hydrolysis of U(VI) occurred and other uranyl complexes, including $UO_2(OH)^+$, $(UO_2)_2(OH)_2^{2+}$ and $(UO_2)_3(OH)_5^{+}$[27] were prevalent. However at pH values >7.0 anionic uranyl species $(UO_2)_3(OH)_7^-$ also coexisted.[28] The lower adsorption rate of uranyl ions at pH values <4 could be attributed to the

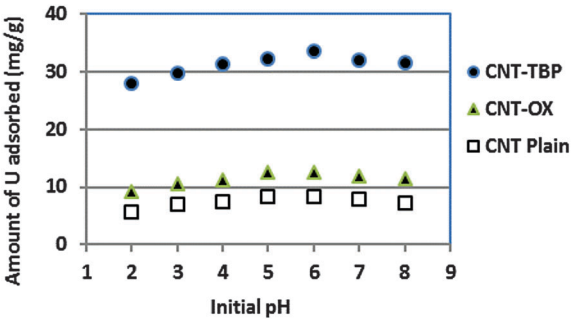

Fig. 9 Effect of initial pH on sorption of U(VI) with CNT-plain, CNT-OX and CNT-TBP.

competition of protons for the active surface of CNTs. Thus adsorption of uranyl ions was found to be maximum at around pH 5 for CNT-TBP and at pH 6 for CNT-OX and CNT plain. At pH > 7 negatively charged uranyl complexes were repelled by the negative surface charge of the sorbent thus resulting in a lower capacity. Due to functionalization of the TBP ligand onto CNTs the amount of uranyl ions adsorbed was found to be higher for CNT-TBP compared to plain and oxidized CNTs.

3.4 Kinetics of sorption

The adsorption of an aqueous solution containing U(VI) on CNT-plain, CNT-OX and CNT-TBP was carried out at pH 5.0 ± 0.1 to investigate the kinetics of sorption. Fig. 10a shows the adsorption process on various sorbents for U(VI) removal. A contact time of 3.0 h was sufficient for the adsorption of uranyl ions onto CNT-TBP to reach equilibrium. However, CNT-plain and CNT-OX reach equilibrium at 3.5 h. The kinetics of U(VI)

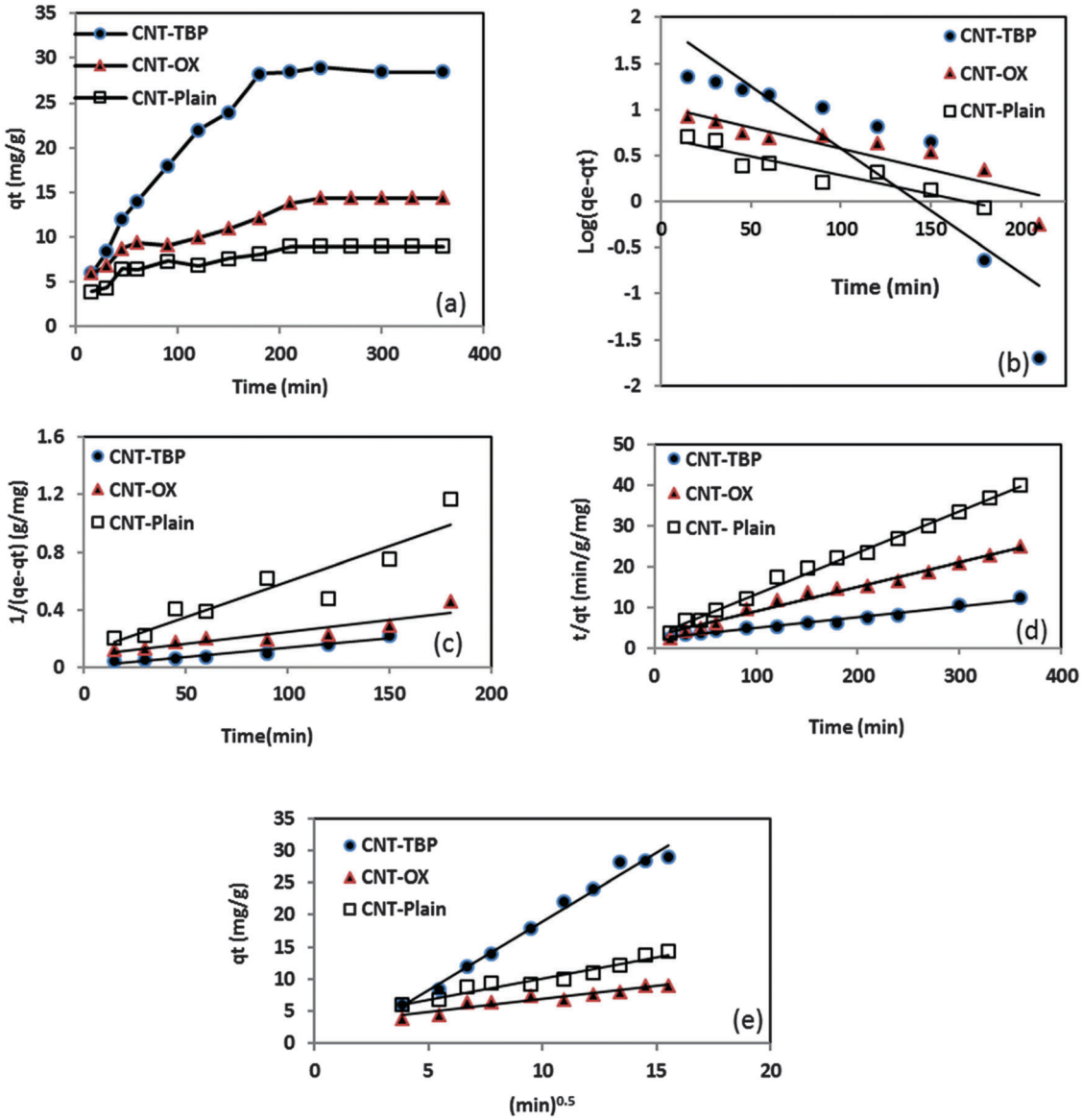

Fig. 10 (a) Equilibration time, (b) pseudo first order kinetics, (c) second order kinetics, (d) pseudo second order kinetics and (e) Web–Morris model of CNT-TBP and U(VI).

Table 4 Kinetic rate constants of the sorption of U(VI) by various CNTs

	Pseudo first order		Second order		Pseudo second order		Web-Morris model	
Adsorbent	K_1 (min^{-1})	R^2	k_2 (mg g^{-1} min^{-1})	R^2	k_2' (mg^{-1} g^{-1} min^{-1})	R^2	k_{int} (mg^{-1} g^{-1} $min^{-0.5}$)	R^2
CNT-plain	0.877	0.870	0.001	0.844	0.0031	0.994	0.670	0.945
CNT-OX	0.004	0.803	0.005	0.859	0.0012	0.981	0.409	0.906
CNT-TBP	0.013	0.800	0.001	0.926	0.0003	0.978	2.147	0.986

adsorption onto all the sorbents prepared were modelled using the Lagergren model[29] or using pseudo first order, second order[30] or pseudo second order models[31] as shown in the following equations:

$$\log(q_e - q_t) = \log q_e - \frac{k_1}{2.303}t \quad (2)$$

$$\frac{1}{q_e - q_t} = \frac{1}{q_e} + k_2 t \quad (3)$$

$$\frac{t}{q_t} = \frac{1}{k_2' q_e^2} + \frac{t}{q_e} \quad (4)$$

where k_L is the Lagergren rate constant of sorption (min^{-1}); k_2 the second-order rate (g mg^{-1} min^{-1}) and k_2' the pseudo-second-order rate constant of sorption (g mg^{-1} min^{-1}); q_e and q_t are the amounts of uranyl ions sorbed (mg g^{-1}) at equilibrium and at a given time t, respectively. The kinetic model plots are shown in Fig. 10b–d. From Table 4, it is evident that among various models, a pseudo second order plot of t/q_t *vs.* t (Fig. 10d) yielded a regression coefficient >0.978. Thus, it could be concluded that the adsorption of uranyl ions with the prepared sorbents followed a pseudo second order kinetic model. Furthermore, the Weber and Morris model[32] describes the intraparticle diffusion between the sorbent and the sorbate. This model correlates the amount of the solute adsorbed and the intraparticle diffusion rate constant (k_{int}) given by the following equation:

$$q_t = k_{int}\sqrt{t} + C \quad (5)$$

It is evident from Fig. 10e that the plot of q_t *vs.* $\sqrt{t}$ yields an intercept and this confirms that in addition to intraparticle diffusion, chemisorptions could also be involved. The values obtained from this model are presented in Table 4.

3.5 Equilibrium studies

Sorption data of uranyl ions with various CNTs were modelled using commonly used isotherms (Fig. 11). The Langmuir model describes the monolayer adsorption and equivalency of the surface adsorption sites. The linear Langmuir model[33] could be expressed as

$$\frac{1}{q_e} = \frac{1}{q_0 C_e K_L} + \frac{1}{q_m} \quad (6)$$

where C_e is the equilibrium concentration (mg L^{-1}) and q_e is the amount of U(VI) sorbed (mg g^{-1}) at equilibrium. The empirical constants b and q_m denote the energy of adsorption and the maximum adsorption capacity, respectively. The results obtained for the various model parameters are listed in Table 5.

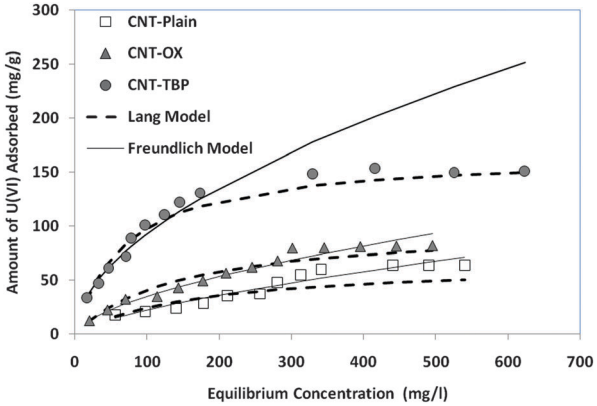

Fig. 11 Adsorption isotherms of various adsorbents with U(VI).

The Langmuir adsorption capacity of the prepared adsorbents towards uranyl ions was in the order of CNT-TBP > CNT-OX > CNT-plain. The adsorption capacity of CNT-TBP was found to be 2.5 times higher than the plain CNTs. The complexing ability of the TBP ligand towards U(VI) resulted in an increased sorption capacity. A comparison of the prepared adsorbents with other functionalized CNTs reported in the literature is given in Table 6. For example, the capacity obtained for CNT-TBP is higher than plain oxidized MWCNTs[28] (43.30 mg g^{-1}), diglycolamide functionalized MWCNTs[34] (133.7 mg g^{-1}), carboxymethyl cellulose grafted CNTs[35] (112.0 mg g^{-1}), imine functionalized carbon spheres[36] (113 mg g^{-1}) and palm shell activated carbon[37] (51.81 mg g^{-1}). A comparison of the adsorption capacities of various functionalized CNTs is given in Table 6. The linear Freundlich model is represented below[38]

$$\log q_e = \frac{1}{n_F}\log C_e + \log K_F \quad (7)$$

K_F and n_F represent the sorption intensity and sorption capacity, respectively. Values of "n_F" ranging between 1 and 10 indicate a good adsorbent. In the present study (Table 5) the 'n' values ranged between 1.445 and 1.835. This signifies the good

Table 5 Isotherm parameters of CNT-plain, CNT-OX and CNT-TBP

	Langmuir model			Freundlich model		
Adsorbent	q_{max} (mg g^{-1})	b (L mg^{-1})	R^{-2}	K_F (L g^{-1})	n_F	R^2
CNT-plain	66.66	0.0057	0.845	0.918	1.445	0.926
CNT-OX	100.00	0.0223	0.985	2.138	1.645	0.981
CNT-TBP	166.66	0.0142	0.972	7.533	1.835	0.964

Table 6 Comparison of the maximum adsorption capacities of various functionalized CNTs towards U(VI) removal

Adsorbent	Maximum adsorption capacity (mg g^{-1})	Reference
Plasma functionalized MWCNTs	66.16	39
Oxidized MWCNTs	43.30	28
Diglycolamide functionalized MWCNTs	133.70	34
Oxidized MWCNTs	33.30	10
Carboxymethyl cellulose functionalized CNTs	112.00	35
Oxidized MWCNTs	45.90	11
Graphene oxide-CNTs	100.0	40
Amidoxime-CNTs	145.0	41
Montmorillonite@C	20.76	42
$CoFe_2O_4$/MWCNTs	212.7	43
CNT-plain	66.66	Present work
CNT-OX	100.00	Present work
CNT-TBP	166.66	Present work

adsorption capabilities of CNT, CNT-OX and CNT-TBP towards the uranyl ion.

3.6 Thermodynamic studies

The feasibility of adsorption was elucidated using thermodynamic parameters like ΔG°, ΔH° and ΔS° which were calculated using the adsorption data. Initially, the constant K_c was calculated using the ratio of U(VI) adsorbed onto the sorbent C_A (g L^{-1}) to that in the aqueous phase at equilibrium C_e (g l^{-1}) given by the following equation:

$$K_C = \frac{C_A}{C_e} \quad (8)$$

Then, ΔG° was determined using the following equation:

$$\Delta G^\circ = -RT \ln K_c \quad (9)$$

where R is the gas constant and T is the temperature in Kelvin. Further, ΔS° and ΔH° were determined using the following Van't Hoff equation:

$$\log K_c = \frac{\Delta S^\circ}{2.303} - \frac{\Delta H^\circ}{2.303RT} \quad (10)$$

A plot of $\log K_c$ *vs.* $1/T$ was obtained for the uranyl ions and the CNT-TBP system (Fig. 12). The thermodynamic parameters namely ΔH° and ΔS° were determined from the slope and intercept, respectively. Table 7 lists the values obtained for various thermodynamic parameters. The negative Gibbs free energy indicated the effectiveness and spontaneity of the sorption process. The endothermic nature of the adsorption process is revealed by the positive enthalpy (ΔH°) values. Positive entropy (ΔS°) values could be due to the dehydration of uranyl ions during adsorption.

3.7 Desorption and recyclability studies

After adsorption of uranyl ions using CNT-TBP as a sorbent, desorption studies of uranium were conducted. It was found that 0.1 M HCl efficiently stripped adsorbed uranium ions. The amount of uranyl ions adsorbed and desorbed for three consecutive cycles using CNT-TBP as a sorbent is shown in Fig. 13. A decreased U(VI) uptake in the order of 11 and 20% were observed at the end of the 1st and 2nd cycles, respectively. Using ordered mesoporous carbon[12] and functionalized activated carbon fibers[9] as adsorbents similar results were observed.

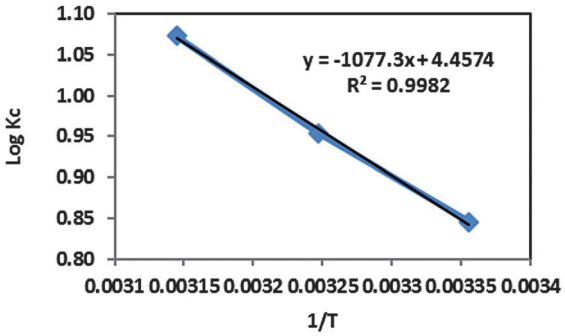

Fig. 12 Thermodynamic studies of CNT-TBP and U(VI) systems.

Table 7 Thermodynamic parameters of CNT-TBP and U(VI)

T (K)	C_e (g L^{-1})	K_c	ΔG (KJ mol^{-1})	ΔS (J mol^{-1})	ΔH [kJ $(mol\ K)^{-1}]^{-1}$
298	12.5	7.00	−4.81		
308	10.0	9.00	−5.63	10.26	20.62
318	7.8	11.82	−6.53		

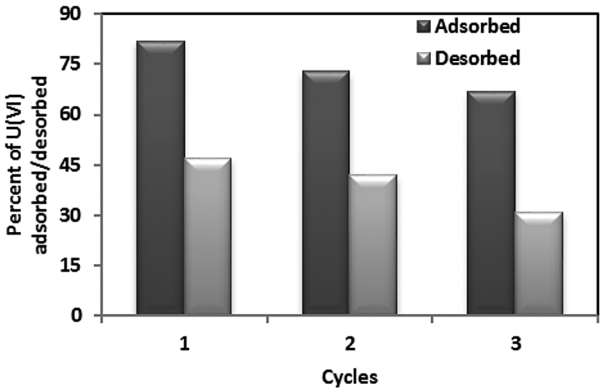

Fig. 13 Desorption and recyclability studies.

4. Conclusions

The chemical vapour deposition technique was used to synthesize carbon nanotubes using ferrocene in benzene as the hydrocarbon source. Ferrocene acted both as a floating catalyst and as a hydrocarbon source. Efficient functionalization was carried out by oxidation with nitric acid and grafting with the tributyl phosphate ligand. FTIR and XPS studies confirmed the presence of a phosphoryl group on CNT-TBP. A pseudo second order model was found to fit the experimental data. A Langmuir adsorption capacity of 166.6 mg g^{-1} was obtained for CNT-TBP with a high regression coefficient. Efficient complexation of U(VI) and the TBP ligand resulted in a high sorption capacity

compared to CNT and CNT-OX. The spontaneity of the reaction was revealed by thermodynamic studies and desorption and recyclability studies were carried out for 3 cycles. FTIR and XPS showed the involvement of the phosphoryl group of the TBP ligand towards the interaction of uranium.

Acknowledgements

The funding received from the Board of Research in Nuclear Sciences, Department of Atomic Energy, Mumbai, India (Ref. No. 2013/36/57-BRNS/2482) to carry out this work is gratefully acknowledged.

References

1 K. Sakr, M. S. Sayed and M. B. Hafez, *J. Radioanal. Nucl. Chem.*, 2003, **256**, 179.
2 T. Ozdemir and A. Usanmaz, *Prog. Nucl. Energy*, 2009, **51**, 240.
3 B. Allard, U. Olofsson and B. Torstenfelt, *Inorg. Chim. Acta*, 1984, **94**, 205.
4 G. M. Naja and B. Volesky, *Toxicity and sources of heavy metals of Pb, Cd, Hg, Cr, As and radionucleides in the environment*, CRC Press, Taylor and Francis Group, USA, 2009, p. 16.
5 WHO, *Guidelines for Drinking Water Quality*, Geneva, 2nd edn, 1998, p. 283.
6 P. D. Bhalara, D. Punetha and K. Balasubramanian, *J. Environ. Chem. Eng.*, 2014, **2**, 1621.
7 M. Caccin, F. Giacobbo, M. Da Ros, L. Besozzi and M. Mariani, *J. Radioanal. Nucl. Chem.*, 2013, **297**, 9.
8 A. M. A. Morsy and A. E. M. Hussein, *J. Radioanal. Nucl. Chem.*, 2011, **288**, 341.
9 S. Mishra, J. Dwivedi, A. Kumar and N. Sankararamakrishnan, *RSC Adv.*, 2015, **5**, 33023.
10 Y. Sun, S. Yang, G. Sheng, Z. Gua and X. Wang, *J. Environ. Radioact.*, 2012, **105**, 40.
11 A. Schierz and H. Zanker, *Environ. Pollut.*, 2009, **157**, 1088.
12 B.-W. Nie, Z.-B. Zhang, X.-H. Cao, Y.-H. Liu and P. Liang, *J. Radioanal. Nucl. Chem.*, 2012, **295**, 663.
13 P. Giridhar, K. A. Venkatesan, T. G. Srinivasan and P. R. Vasudeva Rao, *J. Radioanal. Nucl. Chem.*, 2005, **265**, 31.
14 N. Sankararamakrishnan, D. Chauhan and J. Dwivedi, *Chem. Eng. J.*, 2016, **284**, 599.
15 B. Chen, Z. Zhu, J. Ma, Y. Qiu and J. Chen, *J. Mater. Chem.*, 2013, **1**, 11355.
16 M. Alibrahim and H. Shlewit, *Period. Polytech., Chem. Eng.*, 2007, **51**, 57.
17 V. Datsyuk, M. Kalyva, K. Papagelis, J. Parthenios, D. Tasis, A. Siokou, I. Kallitsisc and C. Galiotis, *Carbon*, 2008, **46**, 833.
18 A. Rossi, F. M. Pirasa, D. Kim, A. J. Gellman and N. D. Spencer, *Tribol. Lett.*, 2006, **23**, 197.
19 S. Van den Berghe, F. Miserque, T. Gouder, B. Gaudreau and M. Verwerft, *J. Nucl. Mater.*, 2001, **294**, 168.
20 S. Chen, J. Hong, H. Yang and J. Yang, *J. Environ. Radioact.*, 2013, **126**, 253.
21 L. L. Burger, in *Physical properties, Science and Technology of Tributyl phosphate*, ed. W. W. Schulz and J. D. Navratil, CRC Press, Boca Raton, Florida, 1984, p. 26.
22 D. F. Peppard and J. R. Ferraro, *J. Inorg. Nucl. Chem.*, 1959, **10**, 275.
23 B. M. Gatehouse, S. E. Livingstone and R. S. Nyholm, *Chem. Soc. Rev.*, 1959, 4222.
24 N. F. Curtis and Y. M. Curtis, *J. Inorg. Chem.*, 1965, **4**, 804.
25 J. R. Ferraro and D. F. Peppard, *Nucl. Sci. Eng.*, 1963, **16**, 389.
26 K. W. Bagnall and M. W. Wakerley, *J. Inorg. Nucl. Chem.*, 1975, **37**, 329.
27 G. Wang, J. Liu, X. Wang, Z. Xie and N. Deng, *J. Hazard. Mater.*, 2009, **168**, 1053.
28 M. Wang, J. Qiu, X. Tao, C. Wu, W. Cui, Q. Liu and S. Lu, *J. Radioanal. Nucl. Chem.*, 2011, **288**, 895.
29 S. Lagergren, *K. Sven. Vetenskapsakad. Handl.*, 1898, **24**, 1–39.
30 Y. S. Ho, D. A. J. Wase and C. F. Forster, *Environ. Technol.*, 1996, **17**, 71.
31 Y. S. Ho and G. McKay, *Advances in Adsorption Separation Science and Technology*, South China University of Technology Press, Guangzhou, 1997, 257.
32 W. J. Weber and J. C. Morris, *J. Sanit. Eng. Div., Am. Soc. Civ. Eng.*, 1963, **89**, 31.
33 I. Langmuir, *J. Am. Chem. Soc.*, 1918, **40**, 1361.
34 A. K. S. Deb, P. Ilaiyaraja, D. Ponraju and B. Venkatraman, *J. Radioanal. Nucl. Chem.*, 2012, **291**, 877.
35 D. Shao, Z. Jiang, X. Wang, J. Li and Y. Meng, *J. Phys. Chem. B*, 2009, **113**, 860.
36 P. S. Dubey, D. A. Dwivedi, M. Sillanpaa, Y.-N. Kwon and C. Lee, *RSC Adv.*, 2014, **4**, 46114.
37 Z.-J. Yi, J. Yao, J.-S. Xu, M.-S. Chen, W. Li, H.-L. Chen and F. Wang, *J. Radioanal. Nucl. Chem.*, 2014, **301**, 695.
38 H. M. F. Freundlich, *J. Phys. Chem.*, 1906, **57**, 385.
39 M. Song, Q. Wang and Y. Meng, *J. Radioanal. Nucl. Chem.*, 2012, **293**, 899.
40 Z. Gu, Y. Wang, J. Tang, J. yang, J. Liao, Y. Yang and N. Liu, *J. Radioanal. Nucl. Chem.*, 2015, **303**, 1835.
41 Y. Wang, Z. Gu, J. Yang, J. Liao, Y. Yang, N. Liu and J. Tang, *Appl. Surf. Sci.*, 2014, **320**, 10.
42 R. Zhang, C. Chen, J. Li and X. Wang, *Appl. Surf. Sci.*, 2015, **349**, 129.
43 L. Tan, Q. Liu, X. Jing, J. Liu, D. Song, S. Hu, L. Liu and J. Wang, *Chem. Eng. J.*, 2015, **273**, 307.